Thermal capillary waves relaxing on atomically thin liquid films

A. M. Willis[a] and J. B. Freund[b),c)]
Mechanical Science and Engineering, University of Illinois at Urbana-Champaign, Urbana, Illinois 61801, USA

(Received 30 July 2009; accepted 22 January 2010; published online 25 February 2010)

Atomistic simulations are used to investigate the relaxation dynamics of thermal capillary waves on thin flat liquid films. Short Lennard-Jones polymers ($n=2$, 4, and 8) model the liquid in films of thickness 6σ to 96σ, where σ is the Lennard-Jones atomic length-scale parameter. Assuming no-slip boundary conditions on the solid wall and constant surface tension and viscosity, the standard continuum model predicts that capillary waves decay with rates ω that scale with wavenumber q as $\omega \sim q^4$ for long wavelengths and $\omega \sim q$ for short wavelengths. The atomistic simulations do indeed show these scalings for ranges of q, and, of course, this model must fail for large q as wavelengths approach atomic scales. However, before a complete breakdown of the continuum description, an unexpected intermediate regime is found. Here the decay rates follow an apparent $\omega \sim q^2$ power law. The behavior in this range collapses for all the cases simulated when q is scaled with the radius of gyration of the polymers, indicating that a molecular-scale effect underlies the relaxation mechanics of these short waves. © *2010 American Institute of Physics*. [doi:10.1063/1.3326077]

I. INTRODUCTION

Thin liquid films (<100 nm) and their dynamics are important in applications such as micron-scale mechanical-electrical systems, cooling devices, biomedical tools,[1,2] microelectronics,[3] and photonics.[4] Under ordinary conditions the motion of the fluid at such scales is, of course, Stokesian, governed by a balance between viscous stresses and pressure gradients, which are generated by external stresses or body forces. However, as films approach molecular scales, the motion of the fluid can also be affected by the fluctuations arising from the thermal energy of the fluid as well as the granular nature of its molecular structure. The interplay between this stress and the Laplace pressure due to surface tension is manifested in dynamic perturbations of a liquid-vapor interface about its equilibrium profile.

There are several cases in which these thermal fluctuations have been shown to play a significant role in small-scale flow dynamics, and they therefore need to be included into models to accurately predict the overall flow behavior. For example, Moseler and Landman[5] demonstrated that a stochastic force must be included in the governing equations in order to qualitatively match the breakup dynamics of a simulated molecular nanometer-scale jet. The neck formed in the breakup of these jets displays a power law that was shown by Eggers[6] to be characteristic of thermal fluctuations coupled to the hydrodynamics. There is also laboratory evidence for such a coupling. In a series of experiments using a colloid polymer, Aarts *et al.*[7] suggested that thermal fluctuations play a key role in the coalescence of droplets. Similarly, Hennequin *et al.*[8] were able to demonstrate that the dynamics of droplet rupture, including the resulting droplet size distribution, is affected by the amplitude of thermal fluctuations on the interface. The necking dynamics of these ruptures also conform to the predictions of Eggers.[6]

There are also theoretical predictions of changes in thin film dynamics due to thermal fluctuations. Davidovitch *et al.*[9] suggest that thermal fluctuations can accelerate the spreading of a fluid drop on a surface and predict a $t^{1/4}$ spreading that is faster than the predicted Tanner's law spreading power law of $t^{1/7}$. This increase in spreading rate has also been recently reported in molecular simulations of spreading.[10] Studying a similar system, Grün *et al.*[11] show that numerical solutions of a stochastic differential equation, which models thermal fluctuations as internally applied stresses, suggest a decrease in the rupture time of unstable thin liquid films by almost an order of magnitude.

Despite the evidence that thermal fluctuations are a necessary component of several nanometer-scale flow phenomena, and that some qualitative features can be reproduced by stochastically augmented continuum models, there exist no direct comparisons that assess the degree to which these equations quantitatively model nanometer-scale fluid flow. This depends upon the scale at which the atomic granularity manifests itself.

Many efforts to assess this have focused on the amplitude and decay rate of thermal capillary waves on thin stable liquid films.[12–19] The dynamics of these waves, as compared with the dynamics in droplet rupture[11] or spreading,[9] have simple hydrodynamic solutions, which facilitate comparisons to models. However, thermal capillary waves are challenging to study experimentally, especially in simple fluids, because of their extremely fast time scales ($\sim 10^{-11}$ s) and short length scales ($\sim 10^{-10}$ m). X-ray spectroscopy is being used in current experimental efforts[12–14,16,19] to resolve the small length scales while complex fluids, such as colloid-polymer systems and thin polystyrene films, are being used to slow down the time scales and increase the length scales of the

[a)]Also at College of Medicine.
[b)]Also at Aerospace Engineering.
[c)]Author to whom correspondence should be addressed. Electronic mail: jbfreund@illinois.edu.

thermal waves. Colloid-polymer systems can have surface tensions 10^6 times smaller than simple fluids,[7,8] which increase the amplitude of the capillary waves. These conditions make colloid polymers useful for phenomenological studies,[7] but it also introduces a fundamental limitation when comparing with theory. Because the film thickness cannot be precisely controlled and fluid properties are complex and undocumented, direct comparisons to continuum models are impossible. Polystyrene films also suffer from similar limitations. Although polystyrene is attractive because of its slow time scales, and unlike colloid polymers particular thicknesses are easy to manufacture, these films exhibit a complex behavior near solid-liquid and liquid-vapor interfaces. The viscoelastic properties of these fluids affect amplitude statistics,[12,13] in cases yielding multiple exponential decay rates for individual wavenumbers.[17] The dynamics may also be altered by absorption of polymer chains onto the solid substrate[19] or changes in the effective viscosity near the surface,[12,20] which also makes it difficult to separate complex material behavior from the general behavior of capillary waves on thin films.

There has been some success in comparing particularly short-chain polystyrene films with Newtonian fluids in thin films.[21] However, the radius of gyration of even these shorter molecules is still an appreciable fraction of the film thickness, which has been shown to have non-Newtonian features.[12,13,19,20] This apparent contradictory evidence highlights the challenge of making conclusive inferences on thin-film behavior from polystyrene films alone.

In the present study, we use idealized but realistic atomistic simulations to provide simple-fluid data for directly assessing the breakdown of the continuum description for the decay of thermal capillary waves. Results are compared with the solutions of the viscous flow equations for the relaxation of thermal capillary waves, e.g., Henle *et al.*[17] The viscous flow predictions are summarized in Sec. II. This is followed by a section describing our model system including the numerical methods used to simulate it. Results are presented in Sec. IV and further discussed in Sec. V.

II. THEORETICAL PRELIMINARIES

Our system is designed so that the thermal capillary waves perturb the stable thickness of the liquid film, as shown schematically in Fig. 1. For convenience the system is assumed to be periodic in both the x and z directions with periods of L and W, respectively. The fluid is assumed to have constant surface tension γ and viscosity η. Its local thickness is $y=h(x,z,t)$. Neglecting any gas-phase dynamics and assuming a small free-surface slope, the Laplace pressure on the liquid side of the interface simplifies to

$$p(x,z,t) = -\gamma\nabla_{2D}^2 h(x,z,t), \tag{1}$$

where ∇_{2D}^2 is the two-dimensional Laplacian in x and z. The surface energy fluctuations associated with the thermal deformation of the free surface should satisfy

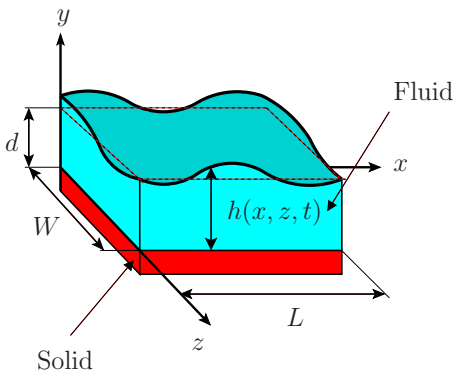

FIG. 1. (Color online) Domain schematic.

$$\langle E\rangle = \tfrac{1}{2}k_B T \tag{2}$$

for each degree of freedom, where k_B is the Boltzmann constant and T is the temperature of the fluid. The energy of a perturbation is modeled as the change in interface surface area due to that perturbation multiplied by the surface tension γ,

$$\langle E\rangle = \left\langle \gamma\int_0^L\int_0^W \sqrt{1+|\nabla h|^2}\,\mathrm{d}x\mathrm{d}z \right\rangle - \gamma LW. \tag{3}$$

The film thickness is decomposed into Fourier modes as

$$h(\mathbf{r},t) = \sum_{\mathbf{q}} h_{\mathbf{q}}(t)\exp(i\mathbf{q}\cdot\mathbf{r}), \tag{4}$$

where $\mathbf{r}$ is a position vector in the x-z plane and $\mathbf{q}$ is the corresponding two-dimensional wavenumber. The sum is over all $\mathbf{q}$ such that

$$\mathbf{q} = \left(\frac{2\pi n_x}{L}, \frac{2\pi n_z}{W}\right) \tag{5}$$

with n_x and n_z integers. Thus, from Eqs. (2)–(4) the mean squared amplitude of each Fourier coefficient $h_{\mathbf{q}}(t)$ must satisfy

$$\langle h_{\mathbf{q}}^2\rangle = \frac{k_B T}{\gamma LW|\mathbf{q}^2|}, \tag{6}$$

so long as γ is constant and interface deformations are small. Although there exist both theoretical results[22] as well as experimental evidence[23,24] that suggest that this model of surface deformation energy fails at scales matching the scales of molecules, such length scales are smaller than the length scales where we observe deviation from the expected relaxation behavior.

A full derivation of capillary wave dynamics can be found in Henle *et al.*,[17] but we will highlight the key assumptions of the model used in our analysis. The flow is assumed to be incompressible ($\nabla\cdot\mathbf{v}=0$) and governed by the Stokes equation

$$\eta\nabla^2\mathbf{v} = \nabla P, \tag{7}$$

where $\mathbf{v}$ is the velocity and P is the pressure. This zero-Reynolds-number approximation will be supported for all perturbations considered in Sec. V. The usual no-slip, no-

penetration conditions at the wall are assumed,

$$\mathbf{v}(y=0)=0, \tag{8}$$

along with a zero-shear-stress condition at the free surface

$$\mathbf{t}\cdot\tau\cdot\mathbf{n}=0, \tag{9}$$

where $\mathbf{t}$ and $\mathbf{n}$ are the interface tangent and normal vectors. τ_{ij} is the Newtonian-fluid stress tensor

$$\tau_{ij}=\eta\left(\frac{\partial v_i}{\partial x_j}+\frac{\partial v_j}{\partial x_i}\right)+\delta_{ij}P. \tag{10}$$

By assuming a small surface perturbation relative to the principal length scale of the flow ($h_q \ll d$ within the long-wavelength lubrication regime and $h_q \ll 1/q$ in the thick-film regime), the leading order form of Eq. (9) is

$$\tau_{12}(y=d)=0. \tag{11}$$

The normal stress condition at the interface is supplied from the Laplace pressure

$$\mathbf{n}\cdot\tau\cdot\mathbf{n}=\gamma\kappa, \tag{12}$$

with κ as the local curvature. This condition, along with Eq. (4), linearizes to

$$\tau_{22}(y=d)=\gamma q^2 h_q(\omega). \tag{13}$$

These assumptions (8)–(13), along with a linearization of the kinematic free-surface condition, yield a prediction for the time correlation behavior of thermally excited surface modes, namely,[17]

$$\langle h_q(t)h_q(0)\rangle=\langle h_q^2\rangle\exp[-\omega(q)t], \tag{14}$$

where the relaxation rate is

$$\omega(q)=\frac{\gamma q^2}{\eta B(q)}, \tag{15}$$

with

$$B(q)=4q\frac{\cosh^2(qd)+q^2d^2}{\sinh(2qd)-2qd}. \tag{16}$$

There are two obvious asymptotic limits of this expression,

$$\omega(q)=\begin{cases}\dfrac{\gamma d^3}{3\eta}q^4, & qd\ll 1\\ \dfrac{\gamma}{2\eta}q, & qd\gg 1.\end{cases} \tag{17}$$

Clearly, $\omega(q)\sim q^4$ corresponds to the long-wavelength lubrication regime while $\omega(q)\sim q$ corresponds to thick films. These are expected to fail as d or disturbances wavelengths $2\pi/q$ approach molecular dimensions. The nature of these failures is investigated with atomistic simulations.

III. ATOMISTIC SIMULATION OF MODEL FLUID FILMS

The atomic interactions in the fluid are modeled with the Lennard-Jones pair potential, which includes a simple $1/r^6$ dispersion (van der Waals) attraction and an empirical $1/r^{12}$ repulsion,

$$u_{\mathrm{LJ}}(r)=\begin{cases}4\varepsilon\left[\dfrac{\sigma^6}{r^6}-\dfrac{\sigma^{12}}{r^{12}}\right], & r\le r_c\\ 0, & r>r_c,\end{cases} \tag{18}$$

where ε is the interaction energy, r is the distance between the two atoms, and σ is the interaction length scale (zero force is at $r=2^{1/6}\sigma$). The simulations employ a cutoff radius $r_c=2.5\sigma$. Most physical properties are insensitive to this r_c, but it does decrease the effective surface tension by about a factor of 2.[25] The Lennard-Jones atoms are joined into polymers using the finite extensible nonlinear elastic potential[26,27]

$$u_{\mathrm{f}}(r)=\begin{cases}-\dfrac{1}{2}kR_o^2\log\left[1-\dfrac{r^2}{R_o^2}\right] & \text{for } r<R_o\\ \infty & \text{for } r\ge R_o,\end{cases} \tag{19}$$

where k is a spring strength and R_o is a bond-length parameter. Taking $k=30\epsilon/\sigma^2$ and $R_o=1.5\sigma$ has been shown to provide realistic packing without imposing any significant new restriction on the numerical time step.[26] In our initial set of simulations, with two-atom molecules making up the fluid, we simulated five films thicknesses: 6σ, 12σ, 24σ, 48σ, and 96σ. If Lennard-Jones parameters for argon were specified, this would correspond to films ranging from 2 to 32 nm thick. Each simulation domain had a length of $L=590\sigma$ and a width of $W=8\sigma$. Results from a $50\sigma\times 50\sigma$ simulation were used to confirm that our results are independent of the simulation domain size (e.g., see Fig. 9). The quasi-one-dimensional $590\sigma\times 8\sigma$ domain used provides lower wavenumber behaviors with little additional computational cost.

The solid substrate is composed of four layers of Lennard-Jones atoms frozen into a face-centered-cubic lattice. The masses and interaction energies of the substrate atoms were ten times that of the fluid to ensure that the wall remained solid. In order to model the stiffness of an extensive solid, the very bottom layer of substrate atoms was held fixed. The velocity-Verlet algorithm was used to advance the equations of motion in time. This method has good but imperfect energy conservation properties, so a weak stochastic Andersen[28] thermostat was applied to the substrate atoms to maintain a constant temperature through the course of the simulation. This thermostat randomly reassigns velocities of substrate atoms, choosing the new velocity from a Boltzmann distribution, with a probability of reassignment of $p=0.005$ each time step. By applying this thermostat just to the substrate, it is not expected to have any effect upon the thermal capillary waves of interest because the surface is not directly influenced by the thermostat.

Fluid parameters were determined independently using established methods[29] with small-scale auxiliary simulations. Viscosity was computed using the Green–Kubo formulation.[29] Similarly, the surface tension was computed in a suspended film configuration[25] with two free fluid-vapor interfaces.

Analyzing the statistics and dynamics of the thermal capillary waves in the atomistic system requires a definition of the interface location based on the atom positions. We base our definition on the density fields constructed by averaging atomic positions every time step in small cubic bins. A

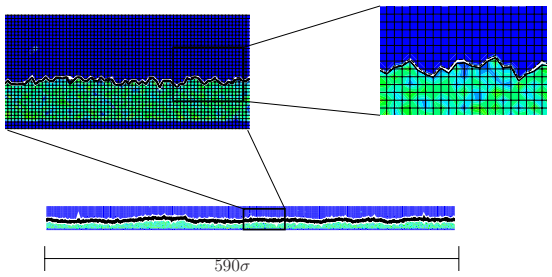

FIG. 2. (Color online) Density fields and interface location defined by the ρ_c isopleths: black $\rho_c=\rho_{\text{bulk}}/6$, white $\rho_c=\rho_{\text{bulk}}/10$, and dashed $\rho_c=\rho_{\text{bulk}}/16$. These lines are superimposed over the density σ^3 bins.

bin volume of σ^3 was used in most calculations, but results are essentially identical for bin volume of $0.02\sigma^3$ for the wavenumbers of interest, as will be seen in Figs. 4 and 5. The surface shape was defined based on atom positions averaged over $\tau_{\text{LJ}}\equiv\sqrt{\sigma m/\epsilon}$. This time scale is on the order of the molecular vibrations and is thus much faster than the relaxation of thermal capillary waves. Averages over $2\tau_{\text{LJ}}$ (also to be seen in Fig. 4) do not alter the results. For each x and z column of bins, the data were interpolated by linear functions to define $\rho(x,y,z,t)$. From this, the interface $y=h(x,z,t)$ is defined by the $\rho(x,y,z,t)=\rho_c=\rho_{\text{bulk}}/10$ isopleth (see Fig. 2). Results are insensitive to ρ_c and the calculated decay rates and amplitudes (see Figs. 4 and 5) are unchanged by values of $\rho_c=\rho_{\text{bulk}}/6$, $\rho_{\text{bulk}}/10$, and $\rho_{\text{bulk}}/16$. This discrete interface is Fourier transformed to $h_{\mathbf{q}}(t)$, and the ensemble averaged time correlations $\langle h_{\mathbf{q}}(t)h_{\mathbf{q}}(0)\rangle$ are computed and fitted to exponentials to calculate $\omega(q)$, as shown in Fig. 3.

A consistent definition of a fluid-vapor interface is an obvious necessity for any study of the dynamics of fluid-vapor interface dynamics. Although we employ a simple cutoff density definition, this definition is not applicable in all fluids.[30–32] The inherent density fluctuations near the fluid-vapor interface found in atomic Lennard-Jones fluids[30,31] as well as liquid gallium interfaces[32] must be included into interface definitions of any fluids that exhibit this behavior. Cutoff density based interfaces of such fluids could mistakenly ascribe the position of a local minimum in these fluctuations as the fluid-vapor interface position and lead to error in measuring interface dynamics. However, the amplitudes of these fluctuations are suggested to be a function of the fluid temperature relative to the critical temperature.[30,31] As will be shown in Sec. V, the fact that for a wide range of fluid temperatures (relative to critical temperature), we see no change in behavior, suggests that local fluctuations in fluid density are not a characteristic of the simulated fluids.

The independence of our interface definition on the numerical parameters of the statistical accumulation of data is

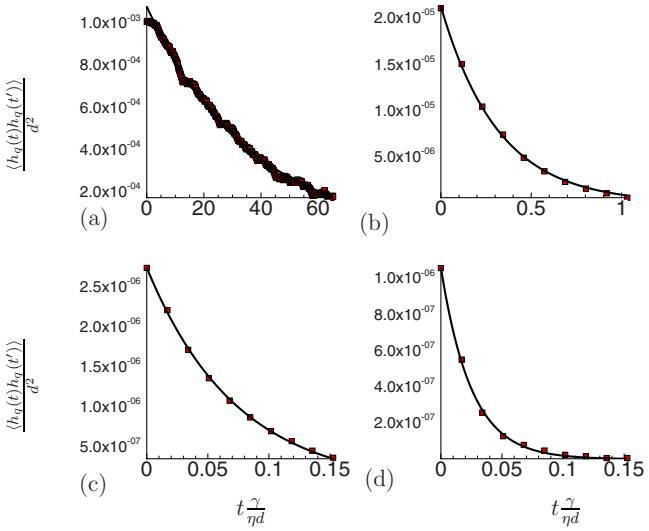

FIG. 3. (Color online) Example exponential fits $e^{-\omega t}$ of $\langle h_q(0)h_q(t)\rangle/d^2$ for the 12σ (4 nm) simulation: (a) $q\sigma=0.05$, (b) $q\sigma=0.32$, (c) $q\sigma=0.95$, and (d) $q\sigma=1.66$.

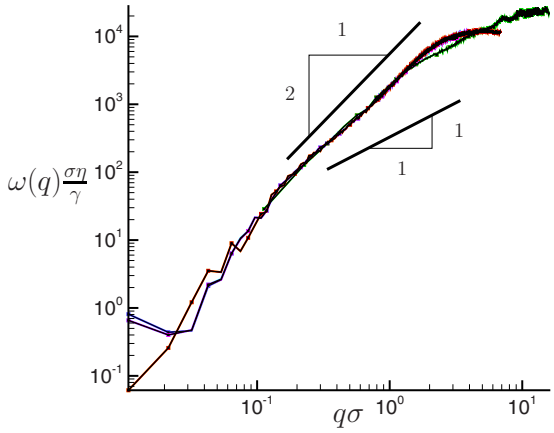

FIG. 4. (Color online) Overlaid curves showing the insensitivity of $\omega(q)$ to seven different sets of numerical averaging parameters for the 12σ (4 nm) fluid film: $\tau_{\text{av}}=\tau_{\text{LJ}}$, $V_{\text{bin}}=\sigma^3$, $\rho_c=\rho_{\text{bulk}}/10$; $\tau_{\text{av}}=2\tau_{\text{LJ}}$, $V_{\text{bin}}=\sigma^3$, $\rho_c=\rho_{\text{bulk}}/10$; $\tau_{\text{av}}=\tau_{\text{LJ}}$, $V_{\text{bin}}=0.5\sigma^3$, $\rho_c=\rho_{\text{bulk}}/10$; $\tau_{\text{av}}=\tau_{\text{LJ}}$, $V_{\text{bin}}=0.25\sigma^3$, $\rho_c=\rho_{\text{bulk}}/10$; $\tau_{\text{av}}=\tau_{\text{LJ}}$, $V_{\text{bin}}=\sigma^3$, $\rho_c=\rho_{\text{bulk}}/6$; $\tau_{\text{av}}=\tau_{\text{LJ}}$, $V_{\text{bin}}=\sigma^3$, $\rho_c=\rho_{\text{bulk}}/16$; and $\tau_{\text{av}}=\tau_{\text{LJ}}$, $V_{\text{bin}}=0.02\sigma^3$, $\rho_c=\rho_{\text{bulk}}/10$. Also included for reference are two solid lines of slopes one and two. The high resolution data ($V_{\text{bin}}=0.02\sigma^3$), which extend to larger q, only deviate for wavelengths approaching the bin size of the $V_{\text{bin}}=\sigma^3$ data.

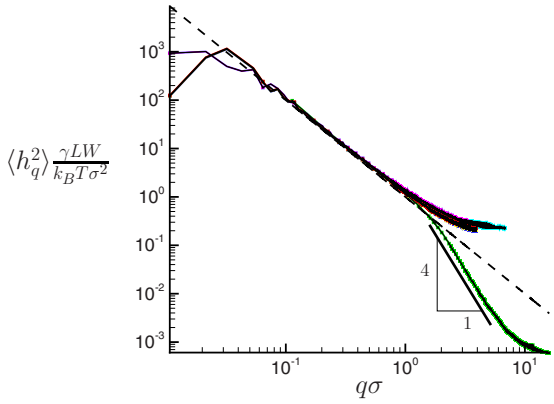

FIG. 5. (Color online) Overlaid curves showing the insensitivity of $\langle h_q^2\rangle$ to seven different sets of numerical averaging parameters for the 12σ (4 nm) fluid film: $\tau_{\text{av}}=\tau_{\text{LJ}}$, $V_{\text{bin}}=\sigma^3$, $\rho_c=\rho_{\text{bulk}}/10$; $\tau_{\text{av}}=2\tau_{\text{LJ}}$, $V_{\text{bin}}=\sigma^3$, $\rho_c=\rho_{\text{bulk}}/10$; $\tau_{\text{av}}=\tau_{\text{LJ}}$, $V_{\text{bin}}=0.5\sigma^3$, $\rho_c=\rho_{\text{bulk}}/10$; $\tau_{\text{av}}=\tau_{\text{LJ}}$, $V_{\text{bin}}=0.25\sigma^3$, $\rho_c=\rho_{\text{bulk}}/10$; $\tau_{\text{av}}=\tau_{\text{LJ}}$, $V_{\text{bin}}=\sigma^3$, $\rho_c=\rho_{\text{bulk}}/6$; $\tau_{\text{av}}=\tau_{\text{LJ}}$, $V_{\text{bin}}=\sigma^3$, $\rho_c=\rho_{\text{bulk}}/16$; and $\tau_{\text{av}}=\tau_{\text{LJ}}$, $V_{\text{bin}}=0.02\sigma^3$, $\rho_c=\rho_{\text{bulk}}/10$. The high resolution data ($V_{\text{bin}}=0.02\sigma^3$) also have a slope of -4 range. These higher resolution data show additional high wavenumber agreement of measured amplitudes with Eq. (6). The dashed line is Eq. (6) and the solid line is for reference.

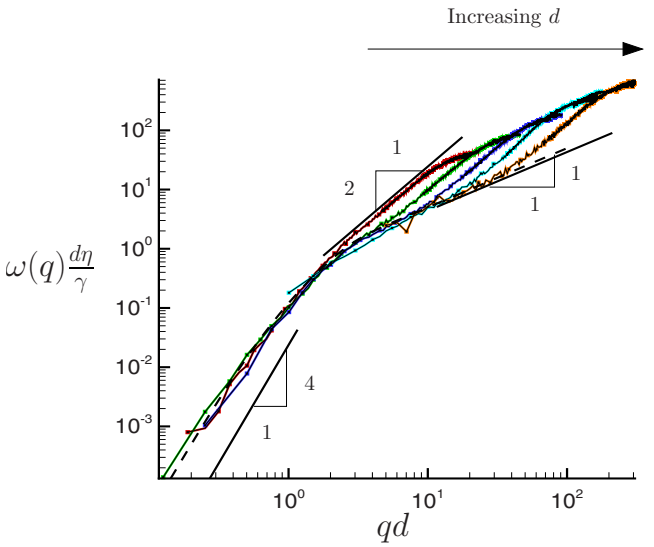

FIG. 6. (Color online) Calculated decay rates $\omega(q)$ as a function of wavenumber amplitude $q=|\mathbf{q}|$ for five films with different thicknesses: 6σ, 12σ, 24σ, 48σ, and 96σ. The dashed line shows Eq. (15).

clearly demonstrated for a wide range of wavenumbers in Figs. 4 and 5. An additional discussion of these different parameters and the consistency of our interface definition is included in Sec. V.

IV. RESULTS

The $\omega(q)$ of all films simulated are plotted in Fig. 6 and compared with Eq. (15). According to Eq. (17), all of the data should collapse onto a curve $\omega\sim q^4$ for small q and a $\omega\sim q$ curve for larger q. The longer wavelengths do indeed asymptote to the $\omega\sim q^4$ line, while all of the films except the thinnest also show a $\omega\sim q$ behavior for larger q. This thinnest film is presumably too thin to be effectively thick even relative to the shortest wavelengths. Unexpectedly, the shorter wavelengths of every film also apparently have its own approximate $\omega\sim q^2$ power law, which is not anticipated by the continuum theory.

With these data scaled by the atomic scale σ, rather than film thickness d, Fig. 7 shows a collapse of the curves in the

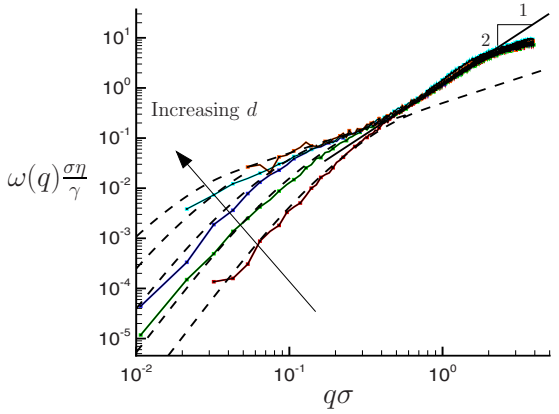

FIG. 7. (Color online) Same as Fig. 6 but here scaled by the Lennard-Jones length scale σ.

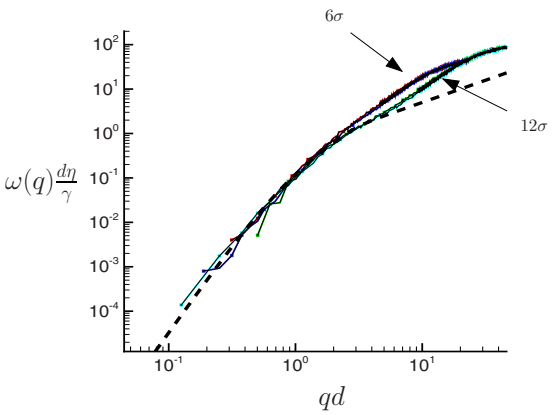

FIG. 8. (Color online) Decay rates of capillary waves for both the 6σ and 12σ films at temperatures $T=0.82\varepsilon/k_B$ and $T=\varepsilon/k_B$. Data are indistinguishable except at small q, where statistical sample size effects are apparent for these simulations.

$\omega\sim q^2$ region, indicative of a molecular scale phenomenon, and thus insensitivity to the film thickness d. To better understand the relevant parameters for new $\omega\sim q^2$ regime, we simulated several other films. The first has an increased temperature from $k_BT=0.83\epsilon$ to $k_BT=\epsilon$. This obviously increases the energy of the perturbations but also decreases both surface tension and viscosity. The decay rates of the thermal capillary waves as functions of q for both 6σ and 12σ are plotted in Fig. 8, along with the data at the lower temperature. The increase in temperature and decrease in surface tension have the expected effect of increasing the mean squared amplitude of the perturbations by 1.8, as predicted by Eq. (6). As shown in Fig. 8, the ω data are independent of temperature. This suggests that interface displacements are not the dominant length scale of the new $\omega\sim q^2$ dynamics and the linear assumption made in Sec. II seems valid.

Figure 9 shows that the $\omega\sim q^2$ region no longer collapses for the σ scaling when different polymer lengths are simulated. However, if the data are scaled by the radius of gyration

$$r_g \equiv \left\langle \sqrt{\frac{1}{N}\sum_{i=1}^{N}(\mathbf{r}_i-\mathbf{r}_{\text{mean}})^2} \right\rangle, \tag{20}$$

the $\omega\sim q^2$ region for the three polymer lengths collapses onto the same power law. In Eq. (20), N is the number of monomers per molecular chain, $\langle\cdots\rangle$ denotes an ensemble average, and $\mathbf{r}_i$ and $\mathbf{r}_{\text{mean}}$ are the position vector of atom i and average position of all atoms in the molecule, respectively. The quantity r_g was measured from bulk samples of each respective polymer. This dependence upon a length scale related to the molecular size of the fluids suggests a molecular-scale granularity effect.

V. SUMMARY AND DISCUSSION

While it is not surprising that the atomistically simulated films show the continuum $\omega\sim q^4$ and $\omega\sim q$ behaviors, it is unexpected that there is a distinct, approximate $\omega\sim q^2$ behavior at short wavelengths. That this collapses to a single curve when scaled by the radius of gyration of the fluid mol-

ecules suggests that dynamics in this new regime depends upon the wavelength of the perturbation relative to the average spatial extent of the fluid molecules, thus suggesting a granular effect, although its specific cause remains unclear.

The wavelength corresponding to the point marked by $\mathbb{R}_{q^2}$ in Fig. 9 is 14σ. This is similar to the length scale at which atomistic fluids are seen to deviate from continuum predictions in confined channel flows, for example. Molecular simulations with simple fluids suggest that Newtonian fluid flow is usually achieved for channel flows with widths greater than 10σ,[33,34] which is comparable in size to the beginning of the $\omega \sim q^2$ regime.

Although we used a simple cutoff density to define our interface, as described in Sec. III, there are some subtleties of a liquid-vapor interface at the molecular level that must be discussed. Tarazona and Chacón[30,31] report intrinsic density fluctuations at the interface of monoatomic Lennard-Jones fluids. These fluctuations are manifestations of molecular ordering near the surface of the fluid and cause obvious concerns for cutoff density based definitions, such as employed in this work. Tarazona and Chacón[30,31] emphasize that these fluctuations were particularly pronounced for atomic Lennard-Jones fluids well below the critical temperature T_c, and as film temperatures approach T_c this molecular ordering near the interface becomes less pronounced and yields smoother intrinsic density profiles.

For the different polymer lengths simulated, our films effectively span a range of T/T_c values. With a $T/T_c \approx 0.70$,[10] the two-atom polymer at $T=\epsilon/k_B$ shown in Fig. 8 has the highest relative temperature, while the $T=0.83\epsilon/k_B$ eight-polymer, which appeared to have no gas phase at this temperature, has a significantly lower T/T_c. Large T/T_c values, such as 0.70, are not expected to show any significant density fluctuations near the fluid-vapor interface.[31] If intrinsic fluctuations in the interface density were affecting the interface measurement, they are expected to be sensitive to T/T_c.[30,31] Since we see no such sensitivity, we conclude they are not a significant factor in this study.

The fluctuations in this new regime are fast, but not fast enough to introduce any obvious inertial effects. Consistent with the viscous continuum model (7), the decorrelation of the surface waves is indeed exponential, as seen in the examples shown in Fig. 3. The fluctuation Reynolds number is also low. For $U=\omega h_q$ and $L=1/q$, $\mathrm{Re}=\rho UL/\eta=0.01$ near the switch from $\omega \sim q$ to $\omega \sim q^2$ behavior at around $q\sigma=0.45$ (see Fig. 9). From Eq. (6), the capillary amplitudes scale as $h_q \sim 1/q$, so the calculated Re should not deviate significantly from this value throughout the quadratic decay regime.

Interestingly, including a slip boundary condition on the wall yields a $\omega \sim q^2$ decay behavior in the long-wavelength limit,[17] but slip can only be significant when the relaxation of the capillary waves is directly affected by the wall, not for wavelengths shorter than those in the $\omega \sim q$ regime. Including slip lengths into the fluid model[17] shifts the lubrication $\omega \sim q^4$, decay rates toward smaller q in an $\omega(q)$ plot such as in Fig. 6. Such a shift would push continuum predictions (dashed line) away from the already well modeled lubrication regime of all of our films. Furthermore, by inspection

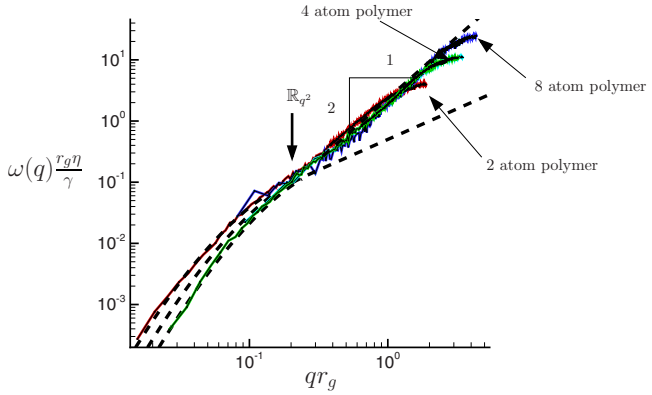

FIG. 9. (Color online) Relaxation rate for r_g scaled data. The four-polymer data are plotted from two simulations with different domain shapes ($8\sigma \times 590\sigma$ and $50\sigma \times 50\sigma$), but these overlay confirming that there is no artifact of the domain shape. The arrow labeled with $\mathbb{R}_{q^2}$ marks a nominal start of the $\omega \sim q^2$ regime.

the velocity of fluid atoms adjacent to the fluid-solid interface revealed no evidence of slip.

It could be suggested that this new behavior is a manifestation of a more viscoelastic nature of the fluid at very fast time scales. Larger size polymers, with radii of gyration greater than half of the film thickness ($d \leq 2r_g$), have shown behavior indicative of viscoelastic properties.[13,19] In a theoretical analysis of several different thin film models, Henle *et al.*[17] showed that a nonslipping viscoelastic fluid's height-height correlations would have multiple exponential decay rates as well as decay rates that are constant relative to wavenumber q. Neither of these features appear in our simulations. As shown in Figs. 3 and 9, the correlations were well fitted by a single exponential decay and measured decay rates showed no q-independent behavior.

It could also be suggested that a deviation in the behavior from the continuum model is related to a wavenumber dependent surface tension $\gamma(q)$. Because surface tension drives the perturbations of the interface back toward equilibrium, a change in the effective surface tension could affect the relaxation rates. At high enough wavenumbers, where wavelengths approach molecule size, molecular deformation as well as interface deformations could store the potential energy of the thermal fluctuations. This consideration was originally included into interface studies by Helfrich[35] and is found to be consistent with both molecular simulations[31] and x-ray spectroscopy.[36] Including bending interactions of molecules into the surface energy of an interface yields an effective surface tension of the form[31,35,36]

$$\gamma(q) = \gamma_o + \kappa q^2 + O(q^4), \tag{21}$$

where κ is a molecular stiffness term to account for energy being stored in molecular bending and γ_o is the large-scale wavenumber independent surface tension. Density functional theory provides an additional consideration for the effective surface tension $\gamma(q)$ of a fluid-vapor interface.[23,37] Mecke *et al.*[23,37] included the nonlocal interactions of the fluid atoms which create a local minimum in $\gamma(q)$ at higher wavenumbers before molecular bending dominated the effective surface tension $\gamma(q) \sim q^2$. However, as is apparent in Fig. 10,

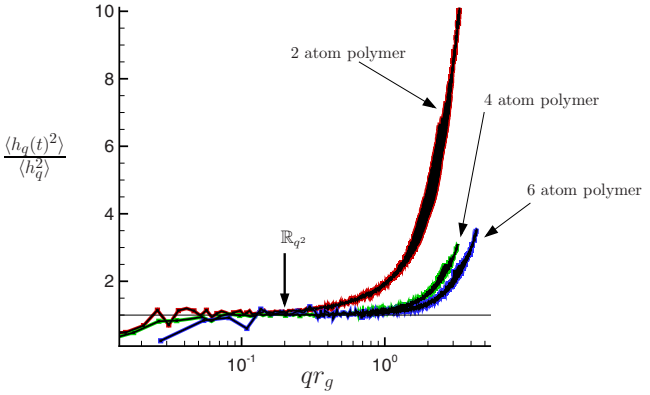

FIG. 10. (Color online) Ratio of the mean-squared amplitude $\langle h_q(t)^2\rangle$ to thermal capillary wave predictions (6) for the different polymer lengths as a function of qr_g. A solid line is drawn at $\langle h_q(t)^2\rangle/\langle h_q^2\rangle=1$, which represents the obvious predictions of Eq. (6). The arrow corresponds to that shown in Fig. 9, marking a nominal beginning of the $\omega\sim q^2$ regime.

the constant surface tension predicts $\langle h_q^2\rangle$ well past the beginning of the approximate $\omega\sim q^2$ behavior. Using higher resolution binning data (Fig. 5), we were able to resolve an apparent transition to a molecular bending regime $\langle h_q^2\rangle\sim 1/q^4$, which occurs at higher wavenumbers than $\mathbb{R}_{q^2}$. The higher resolution binning data did not resolve the predicted localized minimum of Mecke *et al.*; however, our results are consistent with the results from the molecular simulations of Chacón and Tarazona[30,31] who also employed at 2.5σ cutoff radius in their Lennard-Jones fluid simulation. Given that the amplitudes of the thermal capillary waves were consistent with capillary wave theory for $qr_g>\mathbb{R}_{q^2}$ for both the lower resolution binning ($V_{\text{bin}}=\sigma^3$) as well as our higher resolution data ($V_{\text{bin}}=0.02\sigma^3$), there is no reason to believe that wavenumber dependent surface tension explains the apparent $\omega\sim q^2$ regime.

It is noteworthy that the viscosity η and surface tension γ still seem relevant in the new regime. They vary by factors of 7.7 in η and 2 in γ, yet the data still collapse when scaled by these parameters in Fig. 9. The onset of $\omega\sim q^2$ also does not seem to correspond to any obvious failure of the surface tension Laplace pressure model (1), as must occur at molecular scales. We assess this by gauging whether or not the surface energy implied by Eq. (1) obeys equipartition (6). Equipartition must be obeyed, of course, and it indeed is in the atomistic simulations; this test is an indirect assessment of whether or not Eq. (1) provides a reasonable model for the surface energy when $\omega\sim q^2$. In Fig. 9, the $\mathbb{R}_{q^2}$ point, which labels the onset of $\omega\sim q^2$ behavior, does not correspond to a consistent deviation from equipartition for the standard surface tension model, as defined by Eqs. (1) and (6). The two-polymer case does deviate here, but the longer polymers seem to follow Eq. (6) well into the $\omega\sim q^2$ regime. However, as shown in Fig. 5, this apparent breakdown of surface tension in the two-polymer fluid is an artifact of the bin sized use in the $\rho(x,y,z,t)$ calculation and is not present in the higher resolution data.

Given all this, one possibility is that a failure of the applicability of the Newtonian stress tensor (10) at these molecular scales is responsible for the new behavior. The dynamics of thermal capillary waves are a balance of the power dissipated from relaxation of the surface perturbation against the Laplace pressure and the dissipated energy of the flow underneath the fluid surface. Our amplitude results suggest that the Laplace pressure measurements are accurate well into the new regime (Fig. 10). Since the Laplace pressure must be balanced against viscous dissipation in $\text{Re}\to 0$ flows, and our decay rates are faster than expected than under Newtonian dissipation (Fig. 7), the dissipation of the flow near the interface must be less than the expected dissipation under Newtonian assumptions. However, given that there is a collapse of data relative to Newtonian shear viscosity, it is implied that there is a connection between the "new" shear stress and the Newtonian shear stress. Perhaps this connection can be derived from a granular flow treatment similar to that of Haff.[38] Another possibility is that the strain-rate tensor used in the development of Eq. (15) may need to be modified to account for the discrete size of the fluid elements. Thus, rather than assuming a continuous derivative across the velocity field, strain rate may be better modeled as a finite difference between layers of atoms with grid spacing roughly r_g.

It seems that further numerical, experimental, and theoretical investigations are needed to fully explain the observed larger q decay rate behavior. Given that this approximated $\omega\sim q^2$ regime is a function of particle size, it may become apparent at larger, more engineering relevant length scales in fluids with larger molecules.

ACKNOWLEDGMENTS

This research was supported by an allocation of advanced computing resources supported by the National Science Foundation (Grant No. CTS 04-37583). The computations were performed on both Lonestar and Ranger at the Texas Advanced Computing Center. Funding from the National Science Foundation is also gratefully acknowledged.

[1] J. Mendelsohn, S. Yang, J. Hiller, A. Hochbaum, and M. Rubner, "Rational design of cytophilic and cytophobic polyelectrolyte multilayer thin films," Biomacromolecules **4**, 96 (2003).
[2] E. Ostuni, C. Chen, D. Ingber, and G. Whitesides, "Selective depositions of proteins and cells in arrays of microwells," Langmuir **17**, 2828 (2001).
[3] L. L. Lee, C. D. Schaper, and W. K. Ho, "Real-time predictive control of photoresist film thickness uniformity," IEEE Trans. Semicond. Manuf. **15**, 51 (2002).
[4] E. Bormashenko, R. Pogreb, O. Stanevsky, Y. Bormashenko, T. Stein, Y. Z. Gaisin, R. Cohen, and O. V. Gendelman, "Mesoscopic patterning in thin polymer films formed under the fast dip-coating process," Macromol. Mater. Eng. **290**, 114 (2005).
[5] M. Moseler and U. Landman, "Formation, stability, and breakup of nanojets," Science **289**, 1165 (2000).
[6] J. Eggers, "Dynamics of liquid nanojets," Phys. Rev. Lett. **89**, 084502 (2002).
[7] D. G. Aarts, M. Schmidt, and H. N. W. Lekkerkerker, "Direct visual observation of thermal capillary waves," Science **304**, 847 (2004).
[8] Y. Hennequin, D. G. A. L. Aarts, J. H. van der Wiel, G. Wegdam, J. Eggers, H. N. W. Lekkerkerker, and D. Bonn, "Drop formation by thermal fluctuations at an ultralow surface tension," Phys. Rev. Lett. **97**, 244502 (2006).
[9] B. Davidovitch, E. Moro, and H. Stone, "Spreading of viscous fluid drops on a solid substrate assisted by thermal fluctuations," Phys. Rev. Lett. **95**, 244505 (2005).
[10] A. M. Willis and J. B. Fruend, "Enhanced droplet spreading due to thermal fluctuations," J. Phys.: Condens. Matter **21**, 464128 (2009).

[11]G. Grün, K. Mecke, and M. Rauscher, "Thin-film flow influenced by thermal noise," J. Stat. Phys. **122**, 1261 (2006).
[12]H. Kim, Z. Jiang, H. Lee, Y. J. Lee, X. Jiao, C. Li, L. Lurio, M. Rafailovich, and S. K. Sinha, "Hydrodynamic surface fluctuations of polymer films by coherent x-ray scattering," Thin Solid Films **515**, 5536 (2007).
[13]Z. Jiang, H. Kim, X. Jiao, H. L. Y. J. Lee, Y. Byun, S. Song, D. Eom, C. Li, M. H. Rafailovich, L. B. Lurio, and S. K. Sinha, "Evidence for viscoelastic effects in surface capillary waves of molten polymer films," Phys. Rev. Lett. **98**, 227801 (2007).
[14]Z. Jiang, H. Kim, S. G. J. Mochrie, L. B. Lurio, and S. K. Sinha, "Surface and interfacial dynamics of polymeric bilayer films," Phys. Rev. E **74**, 011603 (2006).
[15]S. W. Sides, G. S. Grest, and M. D. Lacasse, "Capillary waves at liquid-vapor interfaces: A molecular dynamics simulation," Phys. Rev. E **60**, 6708 (1999).
[16]B. M. Ocko, X. Z. Wu, E. B. Sirota, S. K. Sinha, and M. Deutsch, "X-ray reflectivity study of thermal capillary waves on liquid surface," Phys. Rev. Lett. **72**, 242 (1994).
[17]M. L. Henle and A. J. Levine, "Capillary wave dynamics on supported viscoelastic films: Single and double layers," Phys. Rev. E **75**, 021604 (2007).
[18]R. L. C. Vink, J. Horbach, and K. Binder, "Capillary waves in a colloid-polymer interface," J. Chem. Phys. **122**, 134905 (2005).
[19]Y. S. Seo, T. Koga, J. Sokolov, M. H. Rafailovich, M. Tolan, and S. Sinha, "Deviations from liquidlike behavior in molten polymer films at interfaces," Phys. Rev. Lett. **94**, 157802 (2005).
[20]W. E. Wallace, D. A. Fisher, K. Efimenko, W. Wu, and J. Genzer, "Polymer chain relaxation: Surface outpaces bulk," Macromolecules **34**, 5081 (2001).
[21]R. Fetzer, M. Rasuscher, R. Seeman, K. Jacobs, and K. Mecke, "Thermal noise influences fluid flow in thin films during spinodal dewetting," Phys. Rev. Lett. **99**, 114503 (2007).
[22]K. R. Mecke and S. Dietrich, "Effective Hamiltonian for liquid-vapor interfaces," Phys. Rev. E **59**, 6766 (1999).
[23]C. Fradin, A. Braslau, D. Smilgies, M. Alba, N. Boudent, K. Mecke, and J. Daillant, "Reduction in the surface energy of liquid interfaces at short length scales," Nature (London) **403**, 871 (2000).
[24]S. Mora and J. Daillant, "X-ray synchrotron study of liquid-vapor interface at short length scales: Effect of long-range forces and bending energies," Phys. Rev. Lett. **90**, 216101 (2003).
[25]A. Trokhymchuk and J. Alejandre, "Computer simulations of liquid/vapor interface in Lennard-Jones fluids: Some questions and answers," J. Chem. Phys. **111**, 8510 (1999).
[26]M. Kröger, W. Loose, and S. Hess, "Rheology and structural changes of polymer melts via non-equilibrium molecular dynamics," J. Rheol. **37**, 1057 (1993).
[27]D. R. Heine, G. S. Grest, and E. B. Webb, "Surface wetting of liquid nanodroplets: Droplet-size effects," Phys. Rev. E **68**, 061603 (2003).
[28]H. Andersen, "Molecular dynamics at constant pressure and/or temperature," J. Chem. Phys. **72**, 2384 (1980).
[29]D. C. Rapaport, *The Art of Molecular Dynamics Simulation* (Cambridge University Press, Cambridge, England, 1997).
[30]E. Chacón and P. Tarazona, "Intrinsic profiles beyond the capillary wave theory: A Monte Carlo study," Phys. Rev. Lett. **91**, 166103 (2003).
[31]P. Tarazona and E. Chacón, "Monte Carlo intrinsic surfaces and density profiles for liquid surfaces," Phys. Rev. B **70**, 235407 (2004).
[32]M. J. Regan, P. S. Pershan, O. M. Magnussen, B. M. Ocko, M. Deutsch, and L. E. Berman, "Capillary-wave roughening of surface-induced layering liquid gallium," Phys. Rev. B **54**, 9730 (1996).
[33]J. J. Magda, M. Tirrell, and H. T. Davis, "Molecular dynamics of narrow, liquid-filled pores," J. Chem. Phys. **83**, 1888 (1985).
[34]J. Koplik and J. R. Banavar, "Continuum deductions from molecular hydrodynamics," Annu. Rev. Fluid Mech. **27**, 257 (1995).
[35]W. Helfrich, "Elastic properties of lipid bilayers: Theory and possible experiments," Z. Naturforsch. **28**, 693 (1973).
[36]J. Daillant and M. Alba, "High-resolution x-ray scattering measurements: I. Surfaces," Rep. Prog. Phys. **63**, 1725 (2000).
[37]K. Mecke and M. Rauscher, "On thermal fluctuations in thin film flow," J. Phys.: Condens. Matter **17**, S3515 (2005).
[38]P. K. Haff, "Grain flow as a fluid-mechanical phenomena," J. Fluid Mech. **134**, 401 (1983).